

Isostructural Salts of the Same Complex Showing Contrasting Thermal Spin-Crossover Mediated by Multiple Phase Changes

**Thomas D. Roberts^a, Marc A. Little^{a,b}, Floriana Tuna^c, Colin A. Kilner^a
and Malcolm A. Halcrow^{a,*}**

*^aSchool of Chemistry, University of Leeds, Woodhouse Lane, Leeds, UK LS2 9JT.
E-mail: m.a.halcrow@leeds.ac.uk*

*^bCurrent address: Department of Chemistry, University of Liverpool, Crown Street, Liverpool,
UK L69 7ZD.*

*^cSchool of Chemistry and Photon Science Institute, University of Manchester, Oxford Road,
Manchester, UK M13 9PL.*

Electronic Supplementary Information

Experimental details

Table S1 Experimental data for the crystal structure determinations of **2^A** and the two organic solvates.

Figure S1 View of the asymmetric unit in **2^A**.

Table S2 Selected bond lengths and angles in the crystal structure of **2^A** and **1^A** at 150 K.

Figure S2 Diagram of **2^A**, showing disorder of the ClO₄⁻ ion between two hydrogen bonding sites.

Figure S3 Packing diagram of **2^A**, showing the layers of interdigitated cations.

Figure S4 View of the asymmetric unit in **2·2CH₃OH**.

Table S3 Selected bond lengths and angles in the crystal structure of **2·2CH₃OH**.

Table S4 Selected bond lengths and angles in the crystal structure of **2·CH₃NO₂·¹/₃(C₂H₅)₂O**

Figure S5 Packing diagrams of **2·2CH₃OH** and **2·CH₃NO₂·¹/₃(C₂H₅)₂O**, showing the cation layers.

Table S5 Hydrogen bond parameters in the crystal structures of **2** and its solvates.

Single crystal X-ray structure investigations of **2·2H₂O**

Table S6 Experimental data for the single crystal structure refinements of **2·2H₂O**

Figure S6 View of the asymmetric unit in **2·2H₂O** at 105 K.

Figure S7 Packing diagram of **2·2H₂O** at 105 K in *P4₁*, showing the layers of interdigitated cations.

Table S7 Selected bond lengths and angles from the refinements of **2·2H₂O** in *P4₁*, illustrating the different spin states of the iron centres at the two temperatures.

Figure S8 Thermogravimetric analyses of **1·2H₂O** and **2·2H₂O**, before and after dehydration.

Figure S9 Variable temperature magnetic susceptibility behaviour of **2·2H₂O**, showing its slow dehydration on repeated scanning above room temperature.

Figure S10 Comparison of the X-ray powder pattern of **2·2H₂O** at room temperature, and a simulation based on the 200 K single crystal structure refinement of **2·2H₂O** in *I4₁/a*.

Figure S11 Comparison of the X-ray powder pattern of **2·2H₂O*** at 200 K, and simulations based on the three different crystal structure refinements of **2·2H₂O** at 200 K.

Figure S12 Comparison of the X-ray powder pattern of **2^B**, and a simulation based on the single crystal structure of **2^A**.

Figure S13 Comparison of the X-ray powder patterns shown by all the different phases of **1** and **2**.

References

Experimental

Ligand *L* and the salt $[\text{FeL}_2][\text{BF}_4]_2 \cdot 2\text{H}_2\text{O}$ (**1**·2H₂O) were synthesised by our previously published procedures.¹ All other reagents and solvents were used as commercially supplied, without further purification.

Elemental microanalyses were performed by the University of Leeds School of Chemistry microanalytical service. IR spectra were run using a Nicolet Paragon 1000 spectrometer, using nujol mull samples held between NaCl windows. Electrospray mass spectra were obtained on a Waters ZQ4000 spectrometer, from MeCN feed solutions. TGA measurements employed a TA Instruments TGA 2050 analyser. Magnetic susceptibility measurements were performed on a Quantum Design SQUID magnetometer, in an applied field of 5000 G. A temperature ramp of 2 K min⁻¹ was used for these measurements, unless otherwise stated. A diamagnetic correction for the sample was estimated from Pascal's constants;² a diamagnetic correction for the sample holder was also applied. Powder X-ray diffraction analyses were performed with a Bruker D8 Advance A25 diffractometer using Cu-K α radiation ($\lambda = 1.5418 \text{ \AA}$). Measurements under vacuum required the samples to be embedded in a nujol mull, leading to weaker diffraction.

Synthesis of $[\text{FeL}_2][\text{ClO}_4]_2$ (2**) and $[\text{FeL}_2][\text{ClO}_4]_2 \cdot 2\text{H}_2\text{O}$ (**2**·2H₂O).** A solution of *L* (0.25 g, 1.05 mmol) and $\text{Fe}[\text{ClO}_4]_2 \cdot 6\text{H}_2\text{O}$ (0.19 g, 0.52 mmol) in MeOH (25 cm³) was stirred until all the solid had dissolved. The resultant solution was filtered, and concentrated to *ca.* 5 cm³. Slow diffusion of diethyl ether vapour into this solution yielded either brown prisms of **2**·2CH₃OH, yellow plates of **2**^A or a mixture of both (see below). Crystallisation vials containing purely **2**^A were collected, and the crystals were ground to a mustard yellow powder. Storage of the sample for 16 hrs under ambient conditions led to a darkening in colour, and afforded analytically pure **2**·2H₂O as a brown powder. Yield 0.28 g, 71 %. Elemental analysis: found C, 40.7; H, 3.80; N, 18.5 %. Calcd for C₂₆H₂₆Cl₂FeN₁₀O₈·2H₂O C, 40.6; H, 3.93; N, 18.2 %. ES mass spectrum: *m/z* 240.1 [LH]⁺, 267.1 [FeL₂]²⁺, 533.2 [FeL₂-H]⁺. IR (nujol): 3588s, 3510m, 3221s, 3130m, 2728w, 1614m, 1578s, 1518m, 1303w, 1286s, 1235m, 1180m, 1159w, 1090br vs, 1024w, 1011m, 977m, 930w, 917w, 848w, 805s, 795s, 747w, 663w, 620m cm⁻¹.

CAUTION. Although we have experienced no difficulties with **2** or **2**·2H₂O at temperatures up to 370 K, metal-organic perchlorates are potentially explosive and should be handled with care in small quantities.

Single crystal X-ray structure determinations

Slow diffusion of diethyl ether into a methanol solution of **2** at room temperature affords either **2**·2CH₃OH (brown prisms), **2**^A (yellow plates) or a mixture of both, while yellow crystals of **2**·*x*CH₃NO₂· $\frac{1}{3}$ (C₂H₅)₂O were similarly grown from a solution of the complex in nitromethane. Experimental data from these structure determinations are given in Table S1. Details of our crystallographic investigations of **2**·2H₂O are given separately below.

All diffraction data were measured using a Bruker X8 Apex II diffractometer, with graphite-monochromated Mo-K α radiation ($\lambda = 0.71073 \text{ \AA}$) generated by a rotating anode. The diffractometer was fitted with an Oxford Cryostream nitrogen low temperature device. The structures were solved by direct methods using *SHELXS97*,³ and developed by full least-squares refinement on *F*² (*SHELXL97*³). Crystallographic figures were prepared using *XSEED*,⁴ which incorporates *POVRAY*.⁵

The asymmetric unit of 2^A contains $\frac{1}{4}$ of a complex dication, with Fe(1) occupying the crystallographic S_4 site [$\frac{1}{4}, \frac{1}{4}, \frac{1}{4}$] and N(2) and C(5) lying on the C_2 axis [$\frac{1}{4}, \frac{1}{4}, z$]; and, half a ClO_4^- anion that is disordered about the C_2 axis [$\frac{3}{4}, \frac{1}{4}, z$]. Three partial environments for this disordered half-anion Cl(12)-O(16) were refined, which shared a common half-occupied Cl atom Cl(12). These were subject to the fixed restraint Cl–O = 1.45(2) Å. No angular restraints were applied to these fragments, and the resultant partial anions deviate significantly from an ideal tetrahedral geometry. The anion disorder means that, on average, each cation forms only two of the four possible N–H...O hydrogen bonds (see Figure S2 below). All wholly occupied non-H atoms were refined anisotropically, and all H atoms were placed in calculated positions and refined using a riding model.

No disorder was detected during refinement of $2 \cdot 2\text{CH}_3\text{OH}$. All non-H atoms were refined anisotropically, while C- and N-bound H atoms were placed in calculated positions and refined using a riding model. The methanolic hydroxy H atoms were located in the Fourier map and allowed to refine with the restraints O–H = 0.90(2) and C...H = 1.90(2) Å, and with displacement parameters of 1.2x those of the attached O atom. The highest residual Fourier peak of $+1.9 e \cdot \text{Å}^{-3}$ is 0.9 Å from Fe(1).

The asymmetric unit of $2 \cdot x\text{CH}_3\text{NO}_2 \cdot \frac{1}{3}(\text{C}_2\text{H}_5)_2\text{O}$ contains three complex cations, six perchlorate anions (two of which are disordered), three nitromethane molecules (one of which is half-occupied) and one molecule of diethyl ether. The disordered anions were modelled over two orientations, with refined occupancy ratios of 0.64:0.36 and 0.56:0.44. These were refined using the restraints Cl–O = 1.39(2) and O...O = 2.27(2) Å. All wholly occupied non-H atoms, plus the part-occupied Cl sites, were refined anisotropically, while H atoms were placed in calculated positions and refined using a riding model. There are six residual Fourier peaks of $>1.5 e \cdot \text{Å}^{-3}$ which all lie within the same disordered anion.

CCDC-936803 (2^A), 936804 ($2 \cdot 2\text{CH}_3\text{OH}$) and 936805 ($2 \cdot x\text{CH}_3\text{NO}_2 \cdot \frac{1}{3}(\text{C}_2\text{H}_5)_2\text{O}$) contain the supplementary crystallographic data for this paper. These data can be obtained free of charge from the Cambridge Crystallographic Data Centre via www.ccdc.cam.ac.uk/data_request/cif.

Table S1 Experimental data for the single crystal structure determinations of phase **2^A** and the two organic solvates.

	2^A	2·2CH₃OH	2·xCH₃NO₂·¹/₃(C₂H₅)₂O
Molecular formula	C ₂₆ H ₂₆ Cl ₂ FeN ₁₀ O ₈	C ₂₈ H ₃₄ Cl ₂ FeN ₁₀ O ₁₀	C _{28.17} H _{31.83} Cl ₂ FeN _{10.83} O ₁₀
<i>M_r</i>	733.32	797.40	808.89
Crystal class	Tetragonal	Monoclinic	Triclinic
Space group	<i>P</i> 4 ₂ / <i>n</i>	<i>P</i> 2 ₁ / <i>n</i>	<i>P</i> $\bar{1}$
<i>a</i> (Å)	9.7396(3)	13.6553(12)	13.1968(7)
<i>b</i> (Å)	–	19.7246(11)	20.4571(12)
<i>c</i> (Å)	18.0080(8)	13.6951(15)	20.6896(12)
α (°)	–	–	86.131(2)
β (°)	–	91.326(5)	75.642(2)
γ (°)	–	–	81.923(2)
<i>V</i> (Å ³)	1708.24(11)	3687.7(6)	5354.3(5)
<i>Z</i>	2	4	6
μ (Mo-K α) (mm ⁻¹)	0.658	0.619	0.642
<i>T</i> (K)	150(2)	150(2)	150(2)
Measured reflections	28726	72389	108015
Independent reflections	2138	7969	21517
<i>R</i> _{int}	0.052	0.100	0.041
<i>R</i> (<i>F</i>) ^a	0.094	0.061	0.078
w <i>R</i> (<i>F</i> ²) ^b	0.348	0.151	0.236
Goodness of fit	1.589	0.912	1.087
Flack parameter	–	–	–

^a $R = \sum[|F_o| - |F_c|] / \sum|F_o|$ ^b $wR = [\sum w(F_o^2 - F_c^2) / \sum wF_o^4]^{1/2}$

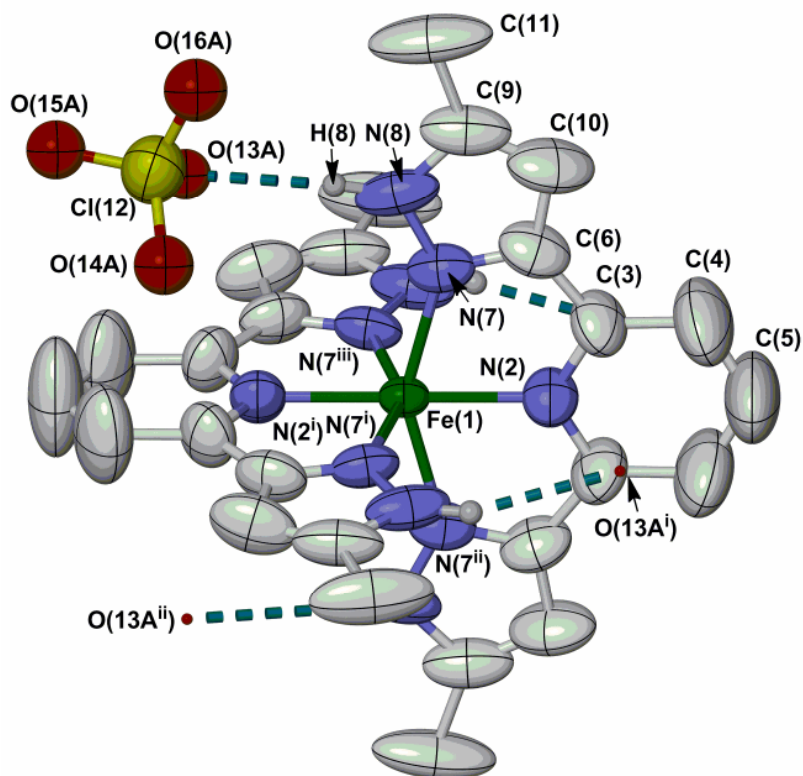


Fig. S1 View of the asymmetric unit in **2^A**. Displacement ellipsoids are at the 50% probability level, and C-bound H atoms have been omitted for clarity. On average, only two of the four possible N–H...O hydrogen bonds in **2^A** are crystallographically occupied, atom O(13Aⁱⁱⁱ) being obscured (Fig. S2). Colour code: C, white; H, pale grey; Cl, yellow; Fe, green; N, blue; O, red.

Symmetry codes: (i) $y, \frac{1}{2}-x, \frac{1}{2}-z$; (ii) $\frac{1}{2}-x, \frac{1}{2}-y, z$; (iii) $\frac{1}{2}-y, x, \frac{1}{2}-z$.

Table S2 Selected bond lengths and angles in the crystal structure of **2^A** (Å, °). See Fig. S1 for the atom numbering scheme employed. Data for **1^A** at the same temperature (150 K) are also presented for comparison.¹

	2^A	1^A
Fe(1)–N(2)	2.031(8)	1.984(6)
Fe(1)–N(7)	2.095(4)	2.033(4)
N(2)–Fe(1)–N(2 ⁱ)	180	180
N(2)–Fe(1)–N(7)	75.62(14)	77.47(12)
N(2)–Fe(1)–N(7 ⁱ)	104.38(14)	102.53(12)
N(7)–Fe(1)–N(7 ⁱ)	93.54(7)	92.70(5)
N(7)–Fe(1)–N(7 ⁱⁱ)	151.2(3)	154.9(2)

^aSymmetry codes: (i) $y, \frac{1}{2}-x, \frac{1}{2}-z$; (ii) $\frac{1}{2}-x, \frac{1}{2}-y, z$.

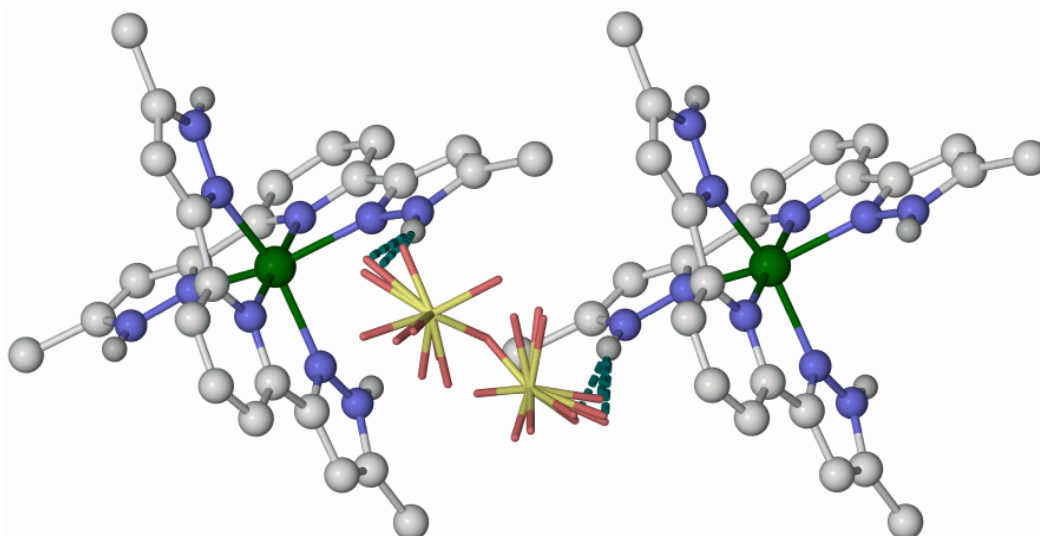


Fig. S2 Diagram of 2^A , showing disorder of the perchlorate ion between two different hydrogen bonding sites. All three anion disorder sites are shown, in both of their orientations across the C_2 axis. C-bound H atoms have been omitted for clarity, and all atoms have arbitrary radii. Colour code: C, white; H, pale grey; Cl, yellow; Fe, green; N, blue; O, red.

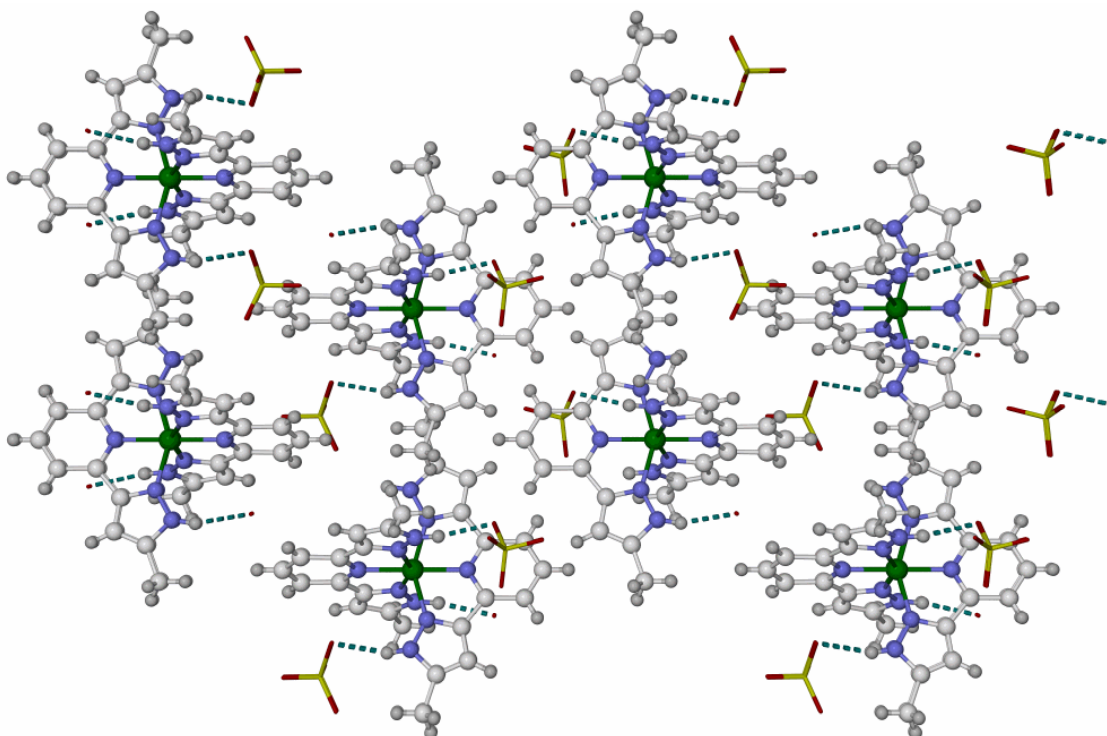


Fig. S3 Packing diagram of 2^A , showing the layers of interdigitated cations. Only one anion disorder site is shown, in one of its orientations across the C_2 axis. All atoms have arbitrary radii, and the ClO_4^- ions are de-emphasised. Colour code: C, white; H, pale grey; Cl, yellow; Fe, green; N, blue; O, red.

The view is perpendicular to the [100] crystal vector, with the unit cell c axis horizontal.

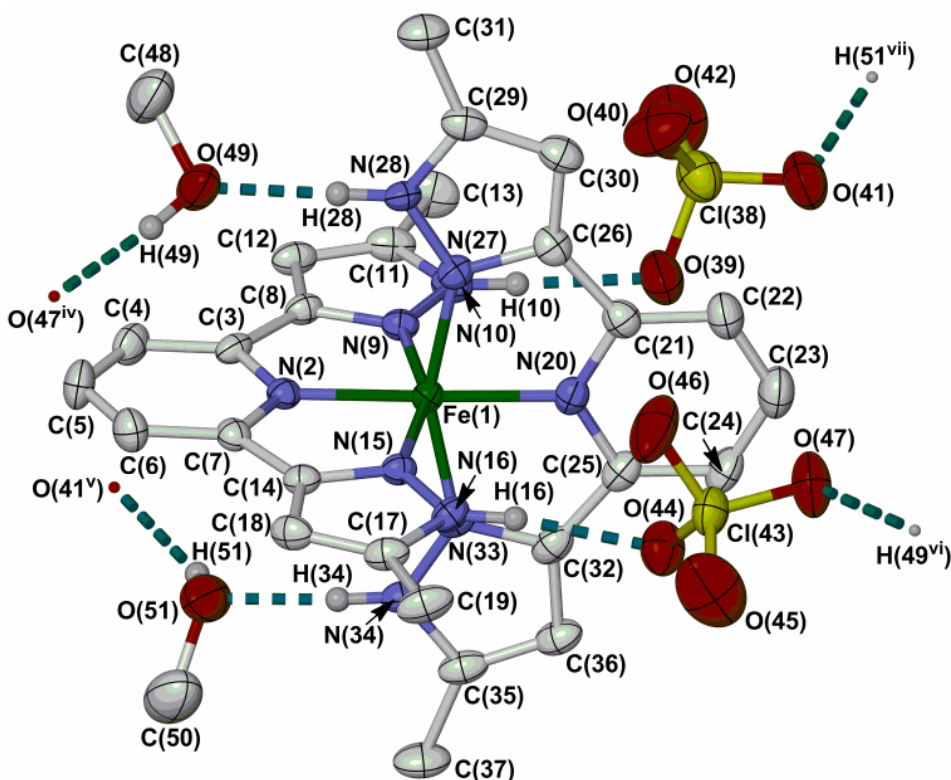


Fig. S4 View of the asymmetric unit in $2 \cdot 2\text{CH}_3\text{OH}$. Displacement ellipsoids are at the 50% probability level, and all C-bound H atoms have been omitted for clarity. Colour code: C, white; H, pale grey; Cl, yellow; Fe, green; N, blue; O, red.

Symmetry codes: (iv) $\frac{1}{2}-x, -\frac{1}{2}+y, \frac{3}{2}-z$; (v) $\frac{3}{2}-x, -\frac{1}{2}+y, \frac{3}{2}-z$; (vi) $\frac{1}{2}-x, \frac{1}{2}+y, \frac{3}{2}-z$;
 (vii) $\frac{3}{2}-x, \frac{1}{2}+y, \frac{3}{2}-z$.

Table S3 Selected bond lengths and angles in the crystal structure of $2 \cdot 2\text{CH}_3\text{OH}$ (Å, °). See Fig. S4 for the atom numbering scheme employed.

Fe(1)–N(2)	1.955(3)	Fe(1)–N(20)	1.955(3)
Fe(1)–N(9)	2.012(3)	Fe(1)–N(27)	1.991(3)
Fe(1)–N(15)	2.018(2)	Fe(1)–N(33)	2.016(3)
N(2)–Fe(1)–N(9)	79.02(11)	N(9)–Fe(1)–N(33)	91.86(11)
N(2)–Fe(1)–N(15)	79.09(11)	N(15)–Fe(1)–N(20)	101.96(11)
N(2)–Fe(1)–N(20)	178.63(11)	N(15)–Fe(1)–N(27)	92.15(11)
N(2)–Fe(1)–N(27)	99.78(11)	N(15)–Fe(1)–N(33)	91.77(11)
N(2)–Fe(1)–N(33)	102.00(11)	N(20)–Fe(1)–N(27)	79.34(12)
N(9)–Fe(1)–N(15)	158.09(11)	N(20)–Fe(1)–N(33)	78.89(12)
N(9)–Fe(1)–N(20)	99.94(11)	N(27)–Fe(1)–N(33)	158.22(11)
N(9)–Fe(1)–N(27)	92.45(11)		

Table S4 Selected bond lengths and angles in the crystal structure of $2 \cdot x\text{CH}_3\text{NO}_2 \cdot \frac{1}{3}(\text{C}_2\text{H}_5)_2\text{O}$ (Å, °).
The atom numbering scheme is the same as that used for $2 \cdot 2\text{CH}_3\text{OH}$ (Fig. S4).

	Molecule A	Molecule B	Molecule C
Fe(1)–N(2)	1.935(3)	2.009(4)	2.051(4)
Fe(1)–N(9)	1.983(4)	2.040(4)	2.100(4)
Fe(1)–N(15)	1.990(4)	2.037(5)	2.097(4)
Fe(1)–N(20)	1.932(4)	2.000(4)	2.058(4)
Fe(1)–N(27)	1.976(4)	2.050(4)	2.096(4)
Fe(1)–N(33)	1.971(4)	2.026(4)	2.098(5)
N(2)–Fe(1)–N(9)	79.00(15)	77.21(18)	75.87(15)
N(2)–Fe(1)–N(15)	78.78(15)	77.18(17)	75.90(15)
N(2)–Fe(1)–N(20)	177.94(15)	171.23(17)	178.05(16)
N(2)–Fe(1)–N(27)	100.59(15)	101.18(15)	103.27(16)
N(2)–Fe(1)–N(33)	101.64(15)	104.47(16)	105.32(16)
N(9)–Fe(1)–N(15)	157.76(15)	154.18(18)	151.75(16)
N(9)–Fe(1)–N(20)	99.01(15)	94.28(17)	105.86(15)
N(9)–Fe(1)–N(27)	93.09(15)	94.11(16)	96.00(15)
N(9)–Fe(1)–N(33)	91.41(15)	90.71(16)	90.63(16)
N(15)–Fe(1)–N(20)	103.22(15)	111.43(17)	102.38(16)
N(15)–Fe(1)–N(27)	91.73(15)	93.97(17)	91.55(16)
N(15)–Fe(1)–N(33)	92.28(15)	92.53(17)	95.65(16)
N(20)–Fe(1)–N(27)	78.93(15)	77.08(15)	75.74(17)
N(20)–Fe(1)–N(33)	78.85(15)	77.43(16)	75.69(17)
N(27)–Fe(1)–N(33)	157.76(15)	154.33(16)	151.40(18)

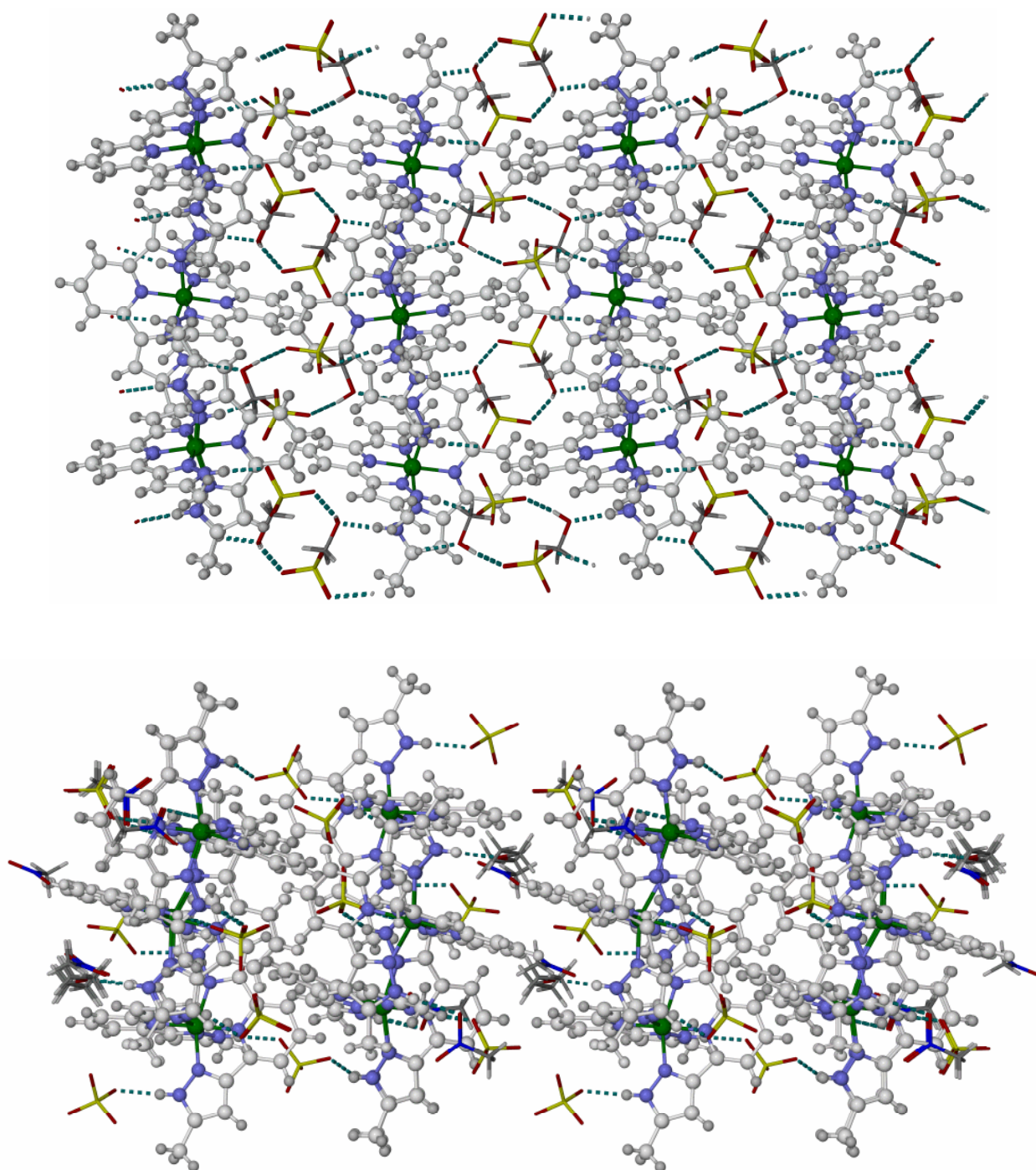


Fig. S5 Packing diagrams of $2 \cdot 2\text{CH}_3\text{OH}$ (top) and $2 \cdot x\text{CH}_3\text{NO}_2 \cdot \frac{1}{3}(\text{C}_2\text{H}_5)_2\text{O}$ (bottom), showing the layers of interdigitated cations. Only one orientation of the disordered residues in the models is shown. All atoms have arbitrary radii, and the ClO_4^- and solvent molecules are de-emphasised.

Colour code: C (complex), white; C (solvent), dark grey; H, pale grey; Cl, yellow; Fe, green; N, blue; O, red. The views are perpendicular to the $[100]$ (top) and $[001]$ (bottom) crystal vectors, with the unit cell b axes horizontal.

Table S5 Hydrogen bond parameters in the crystal structures of **2** and its solvates (Å, °). See Fig. 1 in the main paper for the atom numbering scheme employed. Symmetry codes: (iv) $1/2-x, -1/2+y, 3/2-z$; (v) $3/2-x, -1/2+y, 3/2-z$; ; (viii) $1-x, 1-y, 1-z$.

	D–H	H...X	D...X	N–H...X
2^A, 150 K				
N(8)–H(8)...O(13A)/O(13B)/O(13C)	0.88	2.16/1.92/2.27	3.00(3)/2.78(2)/3.12(11)	160.2/165.2/161.9
2·2CH₃OH				
N(10)–H(10)...O(39)	0.88	1.98	2.859(5)	177.5
N(16)–H(16)...O(44)	0.88	2.06	2.925(4)	167.0
N(28)–H(28)...O(49)	0.88	1.92	2.798(4)	171.7
N(34)–H(34)...O(51)	0.88	1.80	2.675(4)	176.8
O(49)–H(49)...O(47 ^{iv})	0.891(16)	2.205(17)	3.038(4)	155(4)
O(51)–H(51)...O(41 ^v)	0.891(17)	2.193(17)	3.007(5)	152(4)
2·xCH₃NO₂·1/3(C₂H₅)₂O				
N(10A)–H(10A)...O(46)	0.88	1.98	2.847(6)	166.8
N(16A)–H(16A)...O(40)	0.88	1.95	2.817(5)	166.4
N(28A)–H(28A)...O(50)	0.88	1.87	2.752(6)	176.0
N(34A)–H(34A)...O(66A)	0.88	2.02	2.817(9)	150.8
N(10B)–H(10B)...O(57)	0.88	2.08	2.868(8)	148.6
N(16B)–H(16B)...O(51 ^{viii})	0.88	2.27	3.002(8)	141.2
N(28B)–H(28B)...O(75)	0.88	2.03	2.902(6)	173.9
N(34B)–H(34B)...O(60A)	0.88	2.00	2.868(10)	167.8
N(34B)–H(34B)...O(60B)	0.88	2.05	2.881(15)	157.6
N(10C)–H(10C)...O(82)	0.88	1.89	2.763(6)	169.3
N(16C)–H(16C)...O(71)	0.88	2.25	3.029(7)	147.2
N(28C)–H(28C)...O(64B)	0.88	2.08	2.918(11)	159.8
N(34C)–H(34C)...O(54)	0.88	1.89	2.754(10)	166.6

Single crystal X-ray structure investigations of 2·2H₂O

Crystals of 2·2H₂O were obtained by allowing pre-formed crystals of 2^A to stand in air at room temperature for 7 days. The same crystal of 2·2H₂O was examined at three different temperatures (Table S6). Notably, despite the ambiguities described below about the space group of this compound at different temperatures, these crystallographic refinements are of some value. They confirm that the disposition and connectivity of the molecules in 2·2H₂O is identical to that found in 1·2H₂O.¹ They are also consistent with the magnetic susceptibility data in showing that 2·2H₂O has an approximate 1:1 high:low-spin population at 200 K, and is fully low-spin at 105 K (Table S7).

At 300 K the crystal gave the following unit cell: tetragonal *I*, *a* = 13.9733(16), *c* = 36.517(4) Å and *V* = 7130.0(14) Å³. That is consistent with the X-ray powder diffraction data from this material, implying it is isostructural with 1·2H₂O at room temperature (Fig. S10).¹ Attempts to refine the data starting from the structure of 1·2H₂O were only partly successful, however, affording high residuals and substantial disorder in the unique anion site (Table S6). Notably, crystals of 1·2H₂O obtained by hydration of crystalline 1^A behave similarly, after becoming twinned during the hydration process.¹

At 200 K, good refinements were obtained in three space groups: *I*4₁/*a*, and as a racemic twin in *I*4₁ and *P*4₁. While the systematic absences favoured a tetragonal *P* space group, the three refinements are similar in quality and there are indications that the model in *P*4₁ may be in too low symmetry (see below). Moreover, none of the three refinements provided a simulated powder pattern that match the experimental powder diffraction data from the bulk material (Fig. S11). Hence, their validity is uncertain. Attempts to solve the data in the other tetragonal space groups allowed by this descent in symmetry (*P*4₂ and *P*4₂/*n*), and in related monoclinic *C* and triclinic groups, were all unsuccessful.

The asymmetric unit in *I*4₁/*a* contains two unique quarter-cations. The cation centred on Fe(1) lies on the *S*₄ site 0, ¼, ⅛, with N(2) and C(5) on the *C*₂ axis [0, ¼, *z*], while the other cation [Fe(12)] occupies the *S*₄ site ½, ¾, ⅛, with N(13) and C(16) spanning the *C*₂ axis [½, ¾, *z*]. The model also contains one ClO₄⁻ ion and one water molecule lying on general crystallographic positions. The ClO₄⁻ ion is disordered over two equally occupied sites, which were refined using the refined restraints Cl–O = 1.43(2) and O...O = 2.34(2) Å. All non-H atoms were refined anisotropically, and C- and N-bound H atoms were placed in calculated positions and refined using a riding model. The water H atoms were located in the Fourier map, and refined with *U*_{iso} parameters fixed to 1.2x that of O(28).

The asymmetric unit in *I*4₁ contains two unique half-cations lying on the *C*₂ axes ½, ½, *z* [Fe(1), N(2), C(5), N(12), C(15)] and 0, 0, *z* [Fe(22), N(23), C(26), N(33), C(36)]. There are also two ClO₄⁻ ions and two water molecules lying on general crystallographic positions. Both perchlorate ions are disordered, and were refined using the refined restraints Cl–O = 1.46(2) and O...O = 2.38(2) Å. All non-H atoms except the disordered, partial O atoms were refined anisotropically, and C- and N-bound H atoms were placed in calculated positions and refined using a riding model. The H atoms attached to water molecule O(53) were located in the difference map, and allowed to refine freely with a *U*_{iso} parameter fixed at 1.2x that of O(53). The H atoms bound to O(54) were not located, and were omitted from the final least squares cycles. An *ADSYMM* analysis in *PLATON*⁶ of the final refinement suggested transformation into *I*4₁/*a*, as above.

In *P*4₁, the asymmetric unit contains two formula units of the compound, with each residue lying on a general crystallographic site. Two of the four ClO₄⁻ ions were disordered in this model, and were refined over two equally occupied sites sharing a common Cl atom with the refined restraints Cl–O = 1.46(2) and O...O = 2.37(2) Å. All fully occupied non-H atoms were refined anisotropically, and C- and N-bound H atoms were placed in calculated positions and refined using a riding model. Only some of the water H atoms were apparent in the Fourier map, and these did not refine well. So, the water H atoms were not included in the final least squares cycles. Significant correlations between heavy atom parameters in the refinement imply some missing symmetry in the model. Consistent with that, an *ADSYMM* analysis also suggested some missed (pseudo)symmetry elements.⁶ The transformed output model generated by *ADSYMM* in *P*4 was unrealistic, however.

The data at 105 K were solved in $P2_1$, then transformed to $P4_1$ using *ADSYMM*.⁶ The crystal was again refined as a racemic twin, and is in a different setting from the $P4_1$ refinement at 200 K but is otherwise isostructural with it. No disorder was detected during this refinement. All non-H atoms were refined anisotropically, while C- and N-bound H atoms were placed in calculated positions and refined using a riding model. Water H atoms were located in the Fourier map and refined subject to the fixed restraints O–H = 0.90(2) and H...H = 1.47(2) Å, and with thermal parameters equal to 1.2xUeq for the corresponding O atom.

In contrast to the 200 K refinement in this space group, there were no significant correlations between heavy atoms in this refinement that would indicate missing symmetry. However, the lack of powder diffraction data below 130 K means we cannot confirm that this model truly matches the structure of the low-spin material.

Electronic.cif files from these refinements of 2·2H₂O are provided in the Supplementary Information associated with this paper, but they have not been deposited with the CCDC.

Table S6 Experimental data for the single crystal structure refinements of 2·2H₂O (C₂₆H₃₀Cl₂FeN₁₀O₁₀, M_r 769.35).

<i>T</i> (K)	300(2)	200(2)			105(2)
Crystal class	Tetragonal	Tetragonal	Tetragonal	Tetragonal	Tetragonal
Space group	$I4_1/a$	$I4_1/a$	$I4_1$	$P4_1$	$P4_1$
<i>a</i> (Å)	13.9733(16)	13.8945(11)	13.8945(11)	13.8945(11)	13.7315(14)
<i>c</i> (Å)	36.517(4)	36.311(4)	36.311(4)	36.311(4)	36.283(4)
<i>V</i> (Å ³)	7130.0(14)	7010.1(11)	7010.1(11)	7010.1(11)	6841.3(12)
<i>Z</i>	8	8	8	8	8
μ (Mo-K α) (mm ⁻¹)	0.638	0.649	0.649	0.649	0.665
Measured reflections	12068	102553	103766	208125	76680
Independent reflections	3507	7091	13776	27519	20065
R_{int}	0.032	0.040	0.039	0.047	0.042
$R(F)^a$	0.140	0.053	0.049	0.066	0.056
$wR(F^2)^b$	0.306	0.155	0.155	0.241	0.147
Goodness of fit	1.131	1.122	1.025	1.029	1.102
Flack parameter	–	–	0.51(3)	0.49(2)	0.497(14)

$$^a R = \sum[|F_o| - |F_c|] / \sum|F_o| \quad ^b wR = [\sum w(F_o^2 - F_c^2) / \sum wF_o^4]^{1/2}$$

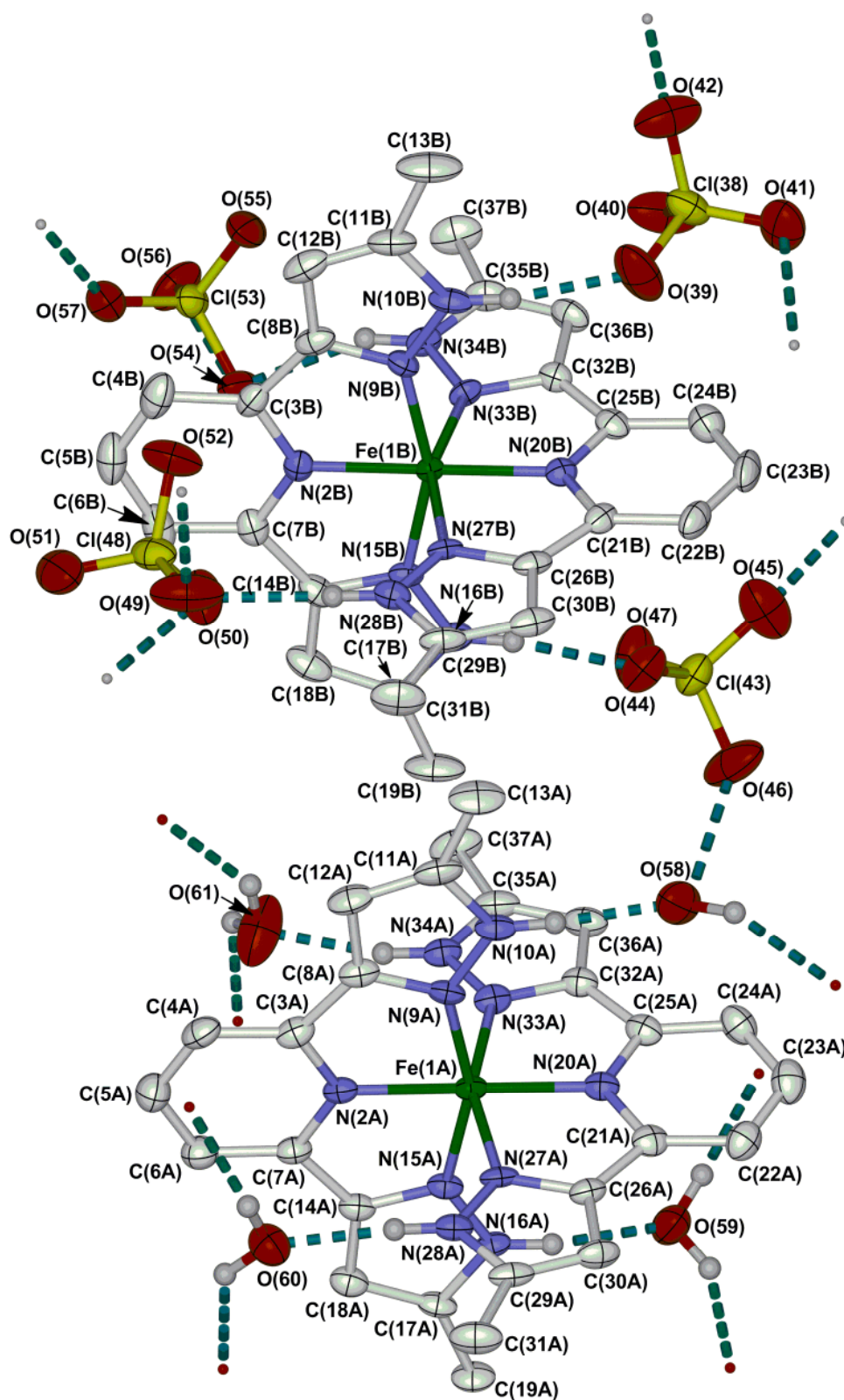


Fig. S6 View of the asymmetric unit in $2 \cdot 2\text{H}_2\text{O}$ in $P4_1$ at 105 K. Displacement ellipsoids are at the 50% probability level, and all C-bound H atoms have been omitted for clarity. Colour code: C, white; H, pale grey; Cl, yellow; Fe, green; N, blue; O, red.

Table S7 Selected bond lengths and angles from the refinements of $2 \cdot 2\text{H}_2\text{O}$ in $P4_1$, illustrating the different spin states of the iron centres at the two temperatures (\AA , $^\circ$). See Fig. S6 for the atom numbering scheme employed.

Temperature	200 K		105 K	
	Molecule A	Molecule B	Molecule A	Molecule B
Fe(1)–N(2)	1.952(5)	2.159(6)	1.935(4)	1.949(4)
Fe(1)–N(9)	2.023(4)	2.198(4)	1.966(3)	1.957(3)
Fe(1)–N(15)	2.025(4)	2.206(4)	1.995(3)	1.988(3)
Fe(1)–N(20)	1.940(7)	2.200(5)	1.935(4)	1.947(3)
Fe(1)–N(27)	2.009(4)	2.212(4)	1.998(3)	2.007(3)
Fe(1)–N(33)	2.015(4)	2.212(4)	1.986(3)	1.971(3)
N(2)–Fe(1)–N(9)	80.02(16)	72.70(14)	78.93(13)	78.95(13)
N(2)–Fe(1)–N(15)	79.66(16)	72.70(14)	79.38(13)	78.88(13)
N(2)–Fe(1)–N(20)	179.5(2)	179.9(2)	179.44(13)	178.72(12)
N(2)–Fe(1)–N(27)	101.91(16)	106.01(15)	100.03(13)	100.14(13)
N(2)–Fe(1)–N(33)	101.90(16)	105.27(14)	101.54(13)	101.86(12)
N(9)–Fe(1)–N(15)	159.7(2)	145.40(19)	158.31(14)	157.83(14)
N(9)–Fe(1)–N(20)	100.01(17)	107.29(15)	100.98(13)	100.01(12)
N(9)–Fe(1)–N(27)	92.93(18)	95.93(17)	91.74(13)	92.20(12)
N(9)–Fe(1)–N(33)	91.42(16)	93.52(16)	92.47(13)	92.14(13)
N(15)–Fe(1)–N(20)	100.32(17)	107.31(15)	100.71(13)	102.17(13)
N(15)–Fe(1)–N(27)	91.43(17)	93.35(16)	91.88(12)	92.10(12)
N(15)–Fe(1)–N(33)	92.57(17)	95.60(17)	91.99(12)	91.97(13)
N(20)–Fe(1)–N(27)	77.61(17)	73.90(16)	79.42(13)	79.11(13)
N(20)–Fe(1)–N(33)	78.58(17)	74.81(16)	79.01(13)	78.88(13)
N(27)–Fe(1)–N(33)	156.2(2)	148.71(18)	158.43(15)	157.99(13)

At 200 K, molecule A is mostly low-spin while molecule B is mostly high-spin. That is consistent with the 1:1 high:low spin-state composition predicted from magnetic susceptibility data ($\chi_{\text{M}}T = 1.79 \text{ cm}^3 \text{ mol}^{-1} \text{ K}$ at 199 K; Fig. 1 of the main paper). At 105 K both molecules are fully low-spin, again in agreement with the susceptibility measurements.

The bond lengths and angles in the higher symmetry refinements of $2 \cdot 2\text{H}_2\text{O}$ at 200 K show only minor differences from those in the $P4_1$ refinement.

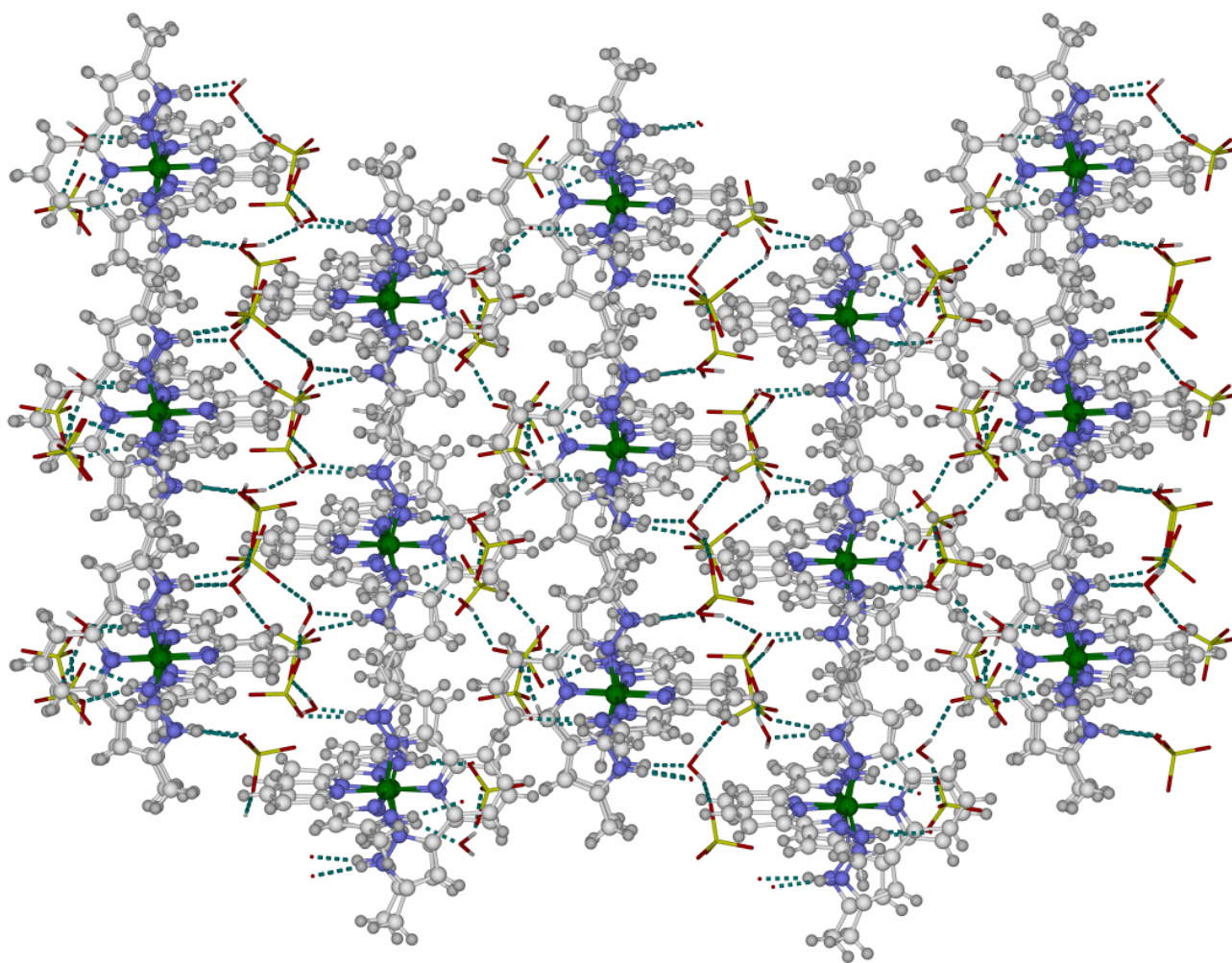


Fig. S7 Packing diagram of $2 \cdot 2\text{H}_2\text{O}$ at 105 K in $P4_1$, showing the layers of interdigitated cations. All atoms have arbitrary radii, and the ClO_4^- ions and water molecules are de-emphasised for clarity. Colour code: C, white; H, pale grey; Cl, yellow; Fe, green; N, blue; O, red.

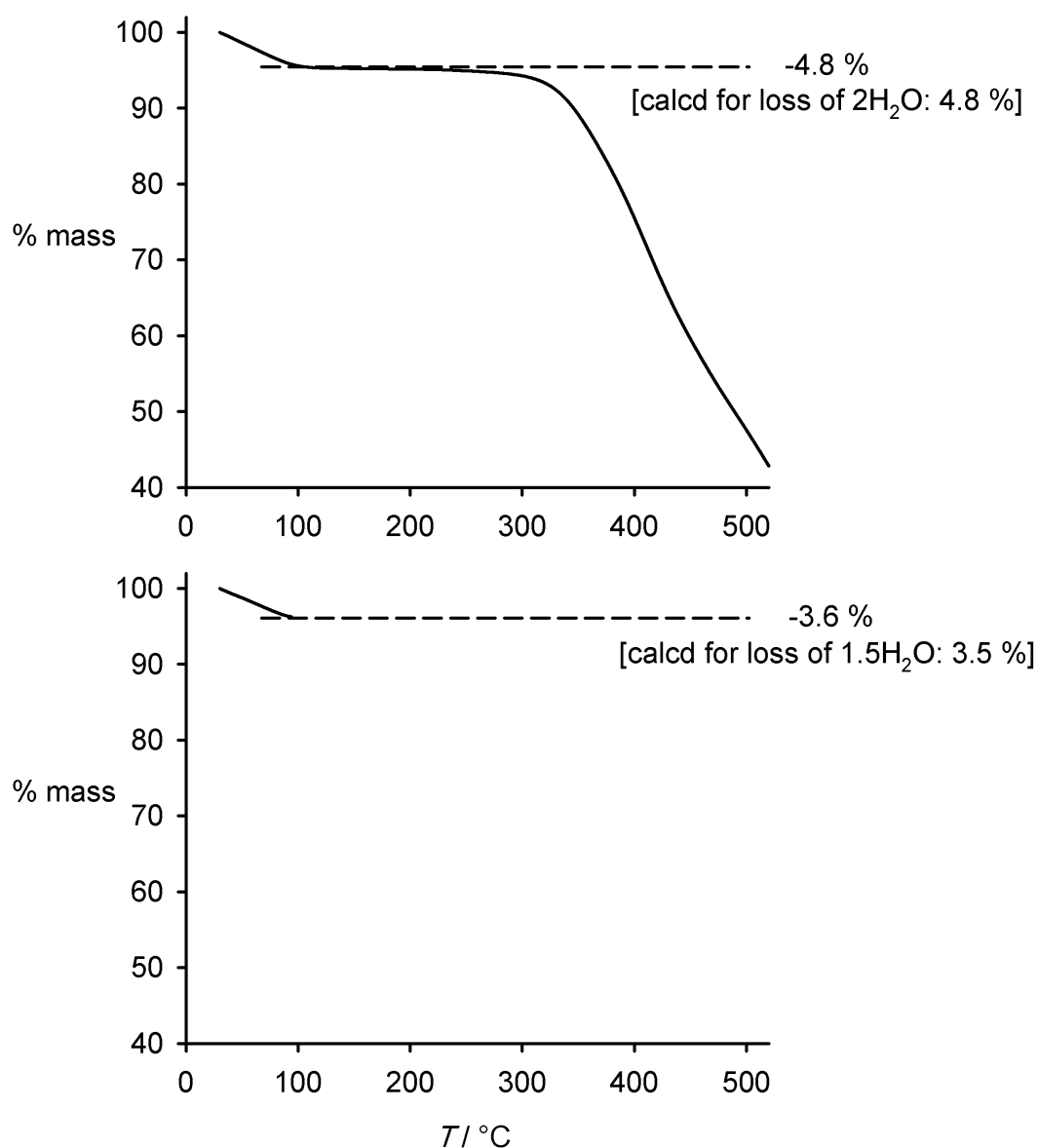


Fig. S8 Thermogravimetric analyses (TGAs) of $1 \cdot 2\text{H}_2\text{O}$ (top) and $2 \cdot 2\text{H}_2\text{O}$ (bottom). Data for $1 \cdot 2\text{H}_2\text{O}$ are taken from ref. 6.

The TGA of $2 \cdot 2\text{H}_2\text{O}$ was only measured to 95°C on safety grounds. For comparison, $1 \cdot 2\text{H}_2\text{O}$ has lost 1.7 equivalents of H_2O (-4.2 % mass) at 95°C.

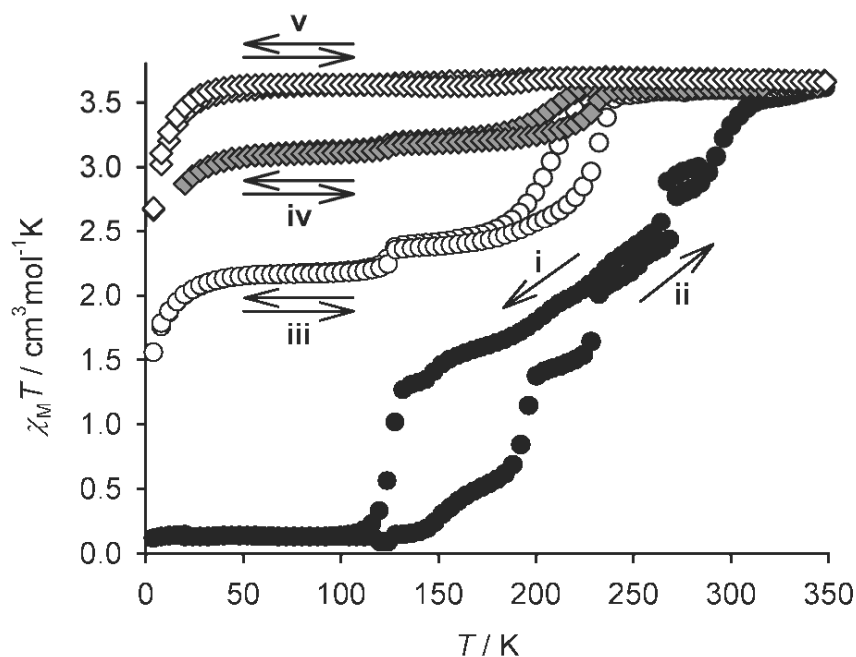


Fig. S9. Variable temperature magnetic susceptibility behaviour of $2 \cdot 2\text{H}_2\text{O}$, showing its slow dehydration on repeated scanning above room temperature.

The sample was: i) cooled from $295 \rightarrow 2$ K (●); ii) warmed from $2 \rightarrow 350$ K (●); iii) cycled between $350 \rightarrow 2 \rightarrow 350$ K (○); iv) cycled again between $350 \rightarrow 20 \rightarrow 350$ K (◇); and v) annealed at 400 K for 2 hrs, then cycled between $350 \rightarrow 2 \rightarrow 350$ K (◇).

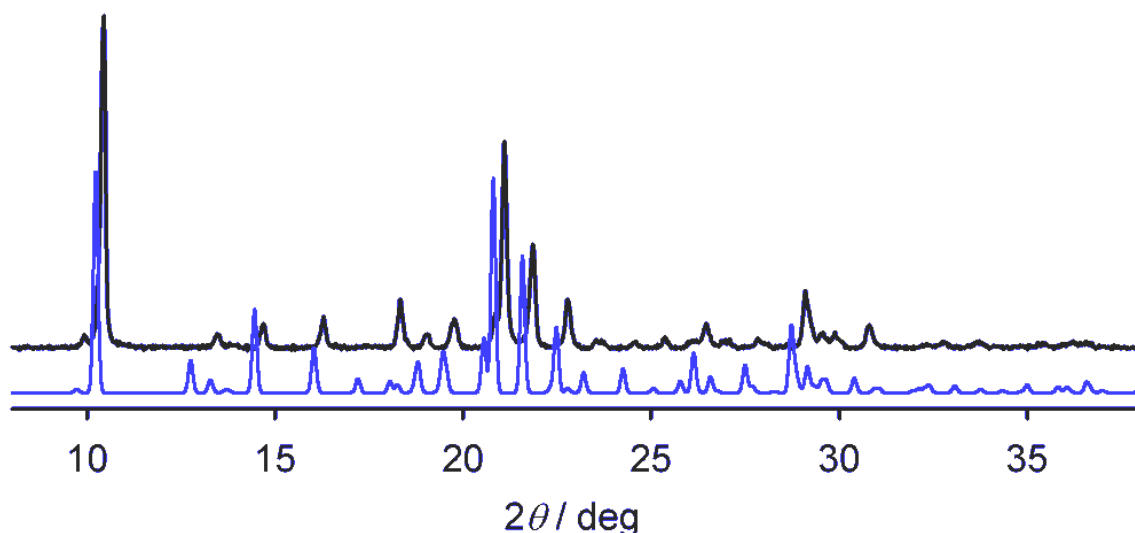


Fig. S10. Comparison of the X-ray powder pattern of $2 \cdot 2\text{H}_2\text{O}$ at room temperature (black), and a simulation based on the 200 K single crystal structure refinement of $2 \cdot 2\text{H}_2\text{O}$ in $I4_1/a$ (blue).

Although the single crystal structure of $2 \cdot 2\text{H}_2\text{O}$ at 300 K could not be refined, the agreement between this powder pattern and the $I4_1/a$ model is excellent [allowing for the difference in temperature, and an offset error in the data]. This confirms that $2 \cdot 2\text{H}_2\text{O}$ is isostructural with $1 \cdot 2\text{H}_2\text{O}$ at room temperature.

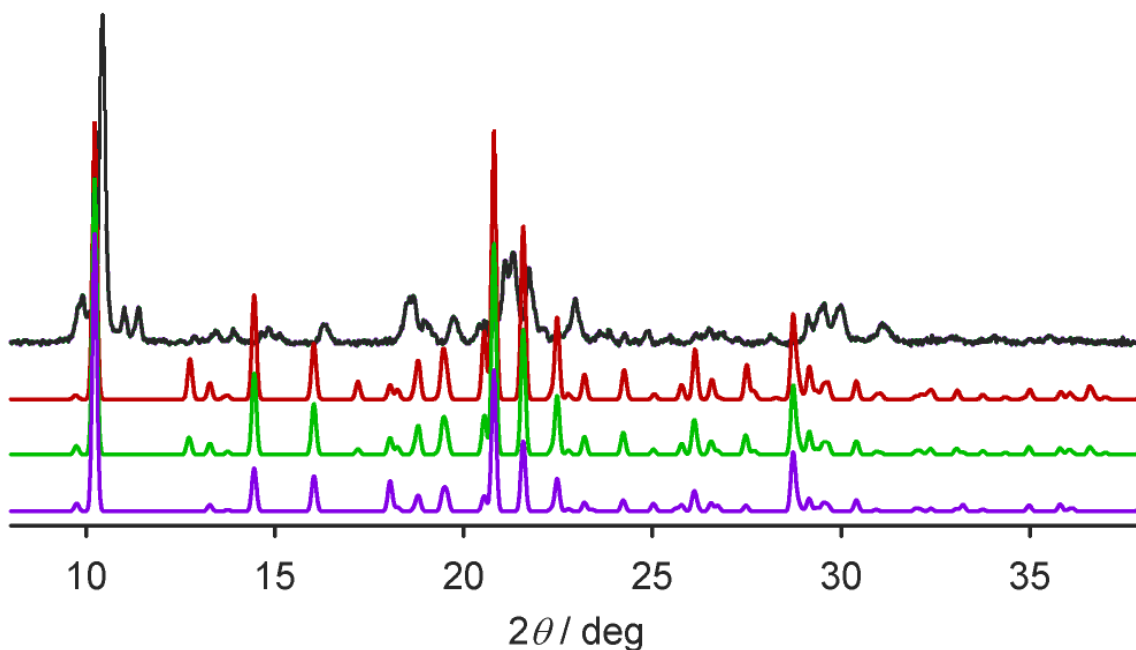


Fig. S11 Comparison of the X-ray powder pattern of $2 \cdot 2\text{H}_2\text{O}^*$ at 200 K (black), and simulations based on the 200 K single crystal structure refinements of $2 \cdot 2\text{H}_2\text{O}$ in $I4_1/a$ (green), $I4_1$ (red), and $P4_1$ (purple).

Despite some similarities, none of these structure solutions reproduces the data, particularly at low angle.

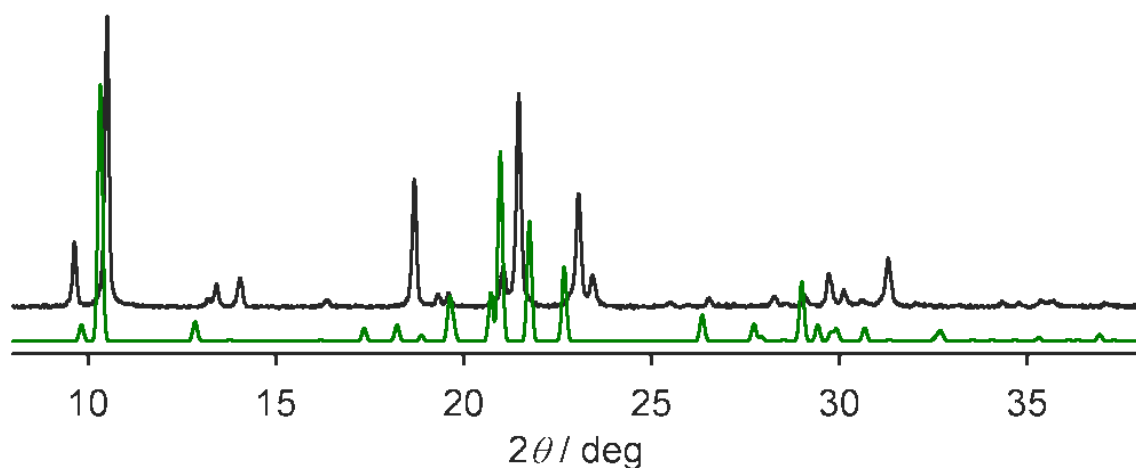


Fig. S12 Comparison of the X-ray powder pattern of 2^B at 300 K (black), and a simulation based on the single crystal structure of 2^A at 150 K (green). Even allowing for the different temperatures, the two phases of anhydrous **2** are clearly not isostructural. Corresponding data for **1** are in ref. 1.

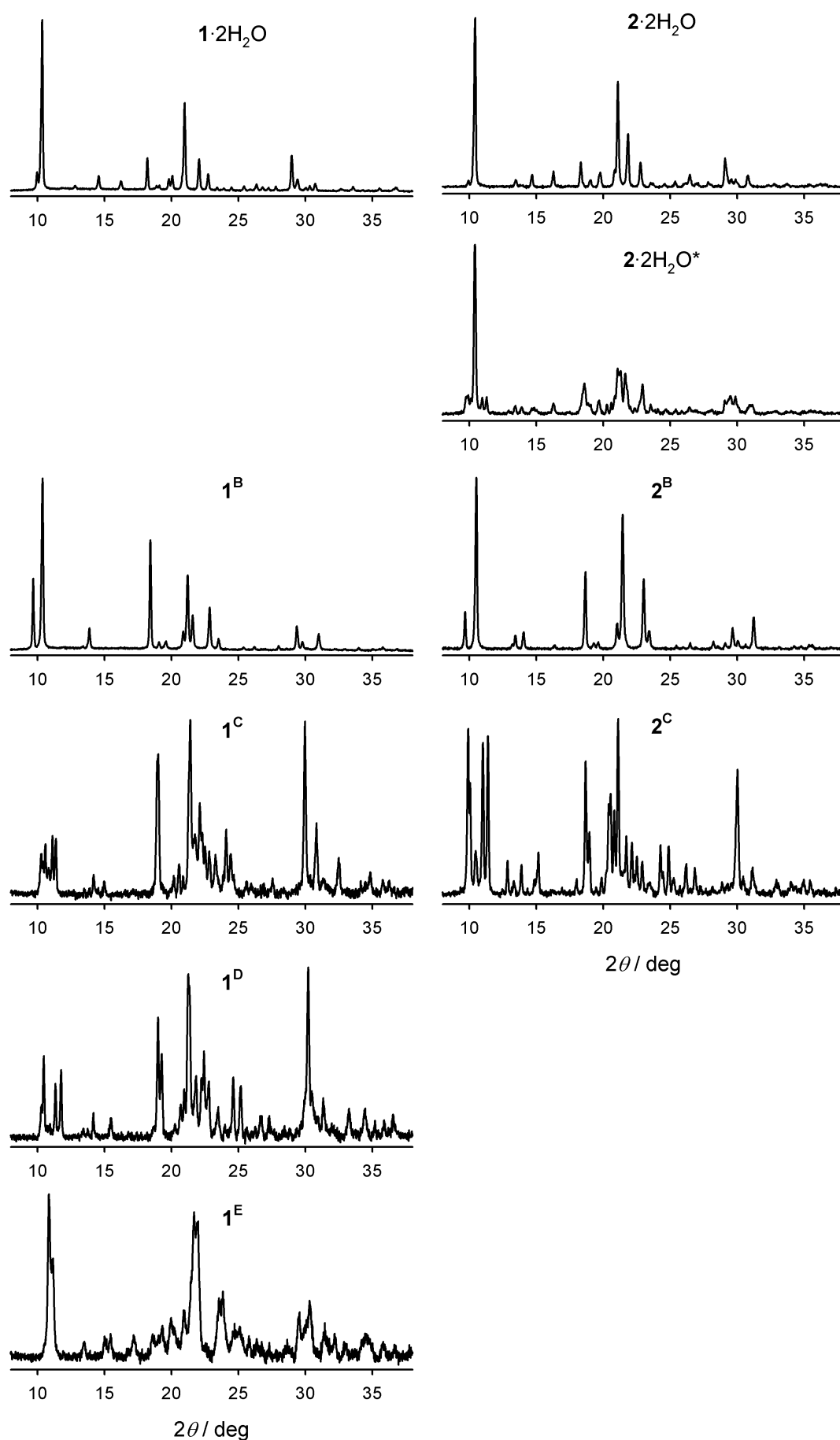


Fig. S13 Comparison of the X-ray powder patterns shown by the different phases of **1** (left) and **2** (right). Data for **1** are taken from ref. 1. The powder patterns for **1^C-1^E** and **2^C** are noisier because they were obtained from nujol mull samples.

References

1. T. D. Roberts, F. Tuna, T. L. Malkin, C. A. Kilner and M. A. Halcrow, *Chem. Sci.*, 2012, **3**, 349.
2. C. J. O'Connor, *Prog. Inorg. Chem.*, 1982, **29**, 203.
3. G. M. Sheldrick, *Acta Crystallogr., Sect. A*, 2008, **64**, 112.
4. L. J. Barbour, *J. Supramol. Chem.*, 2001, **1**, 189.
5. *POVRAY*, v.3.5, Persistence of Vision Raytracer Pty. Ltd., Williamstown, Victoria, Australia, 2002 (<http://www.povray.org>).
6. A. L. Spek, *J. Appl. Crystallogr.*, 2003, **36**, 7.